The dynamics of hinge flexibility in receptor bound immunoglobulin E revealed by electron microscopy

Rasmus K Jensen[1,3], Michaela Miehe[2], Rosaria Gandini[1], Edzard Spillner*, and Gregers R Andersen*[1]

[1] Department of Molecular Biology and Genetics, Aarhus University, Universitetsbyen 81, DK-8000 Aarhus, Denmark

[2] Immunological Biotechnology, Department of Biological and Chemical Engineering, Aarhus University, Gustav Wieds Vej 10C, DK-8000 Aarhus, Denmark

[3] Structural and Computational Biology Unit, European Molecular Biology Laboratory, Heidelberg, Germany.

*Corresponding authors. Email: e.spillner@eng.au.dk; gra@mbg.au.dk

Abstract

Immunoglobulin E is a mammal specific antibody isotype supporting the immune response against parasites and venoms, but also a driver of allergic responses. Structural and biophysical studies have defined the conformation of the IgE Fc fragment bound to the cell surface receptor FcεRIα and the dynamic properties of the IgE Fc. How these prior studies translate to the full antibody-receptor complex remains unknown. Here we show that IgE bound to the FcεRIα adopts two distinct defined conformations. In a cryo-EM structure of the IgE FcεRIα complex, IgE adopts a T-like conformation where the antigen binding Fab arms may be parallel to the cell membrane. A second Y-like conformation captured in negative stain EM features a different arrangement with two Fab arms likely to orient away from the membrane. Solution studies suggest the two receptor bound IgE conformations to be present in a 2:1 ratio. Introduction of flexibility in the Fab-Fc hinge diminishes the biological activity of IgE demonstrating a functional role for the observed defined Fab-Fc hinge conformations.

Introduction

Immunoglobulin E (IgE) has a key role in allergic diseases and is found both in the circulation and on a variety of cell types (Broide, Finkelman et al., 2011). It interacts directly with the high-affinity receptor FcεRI and the low-affinity receptor CD23 (Gould & Sutton, 2008). Upon crosslinking by allergens, FcεRI-bound IgE on mast cells and basophils triggers degranulation, release of mediators, and immediate reactions (Gould & Sutton, 2008) (Fig. 1A). Crosslinking of IgE-FcεRI complexes by antigens (which may be allergens) induces FcεRI signal transduction through receptor clustering (Shelby, Holowka et al., 2013). The cytoplasmic domains of the FcεRI β- and γ-subunits contain ITAM motifs that are phosphorylated upon FcεRI crosslinking and link to downstream signaling pathways starting with activation of the Lyn and Syk kinases (Kraft & Kinet, 2007). The homotrimeric CD23 is expressed by epithelial cells, B cells and myeloid cells (Galli & Tsai, 2012) and is crucial for facilitated antigen presentation, transport across the epithelium, amplification of IgE production and epitope spreading (Clement, Fortune et al., 2006, Gould & Sutton, 2008) (Fig. 1A).

Antibodies are commonly perceived as flexible molecules due to the presence of a hinge region connecting the antigen recognizing Fab fragment to the constant Fc fragment (Burton, 1990). But the hinge region in IgE is short compared to the IgG isotypes and furthermore the IgE epsilon heavy chain contains four constant domains as compared to three constant domains in IgG (Fig. 1B). The short hinge region in IgE is expected to reduce flexibility compared to IgG (Gould, Sutton et al., 2003, Sutton & Davies, 2015) and experimental evidence for limited rotational freedom at the Fab-Fc hinge in both free and FcεRI bound IgE was early on demonstrated by spectroscopy (Zheng, Shopes et al., 1992) and the formation of 2D crystals of IgE on hapten covered mono- and bilayers (Uzgiris, 1987). There is, however, an understanding of the IgE Fabs as being somewhat flexible relative to the Fc (Drinkwater, Cossins et al., 2014, Hunt, Keeble et al., 2012, Roux, Strelets et al., 1998). A number of structural studies have investigated the conformational properties of the IgE Fc (Fig. 1B), but little structural work has been done on the full IgE molecule. We recently showed that at the resolution of negative stain EM (ns-EM), the Fabs appears to be rigidly associated with the Fc in intact free IgE and

in IgE bound to the monoclonal antibody ligelizumab (Jensen, Jabs et al., 2020). Prior structural studies using the Fc fragment as a proxy for the full IgE have provided crucial information regarding the fundamental intermolecular interaction between antibody and receptor but these structures do not take into account the effect of the Fab arms (Garman, Wurzburg et al., 2000, Holdom, Davies et al., 2011).

Results

Cryo-EM analysis reveals a T-shaped IgE in complex with FcεRIα

To determine an atomic structure of the full IgE bound to the FcεRI receptor, we prepared the complex between the 170 kDa IgE HMM5 and the 50 kDa FcεRIα ectodomain. Cryo-EM grids prepared using standard methods led to strong preferential orientation of the complex, presumably due to interaction with the air-water interface (Glaeser, 2018). To overcome this complication, we prepared samples on self-wicking Quantifoil Active grids using the Chameleon device (Darrow, Moore et al., 2019). Though preferential orientations were still present, we were able to resolve the structure to an overall resolution of 4.1 Å (Fig. 1C-D and supplementary Fig. 1A-C). In this consensus map extending over the full complex, the two Fab arms are positioned asymmetrically with respect to the Fc and the receptor (Fig. 1D), with a proximal Fab located close to the Fc, and a distal Fab sitting slightly further away from the Fc.

In contrast to the Fab arms, the IgE Fc and its interface with FcεRI is well resolved and focused refinement on these domains yielded a 3D reconstruction with a resolution of 3.8 Å (Fig. 1E and supplementary Fig. 1D). An atomic model for the IgE-FcεRI complex was first obtained by model building and refinement against the focused map which allowed side-chain level modelling in most regions (Fig. 1F-I). The model was subsequently extended using the consensus map to contain the constant domains Cε1 in the heavy chain and CL in the light chain of the two Fab arms. For both Fab-Fc hinges, there is density for the linker between the Cε1 and Cε2 domains (supplementary Fig. 2A).

The densities for the two Cε1 domains are less well-resolved than their connected Cε2 domains and the local resolution of the Cε1 and the associated CL domains is 7-10 Å (supplementary Fig. 1E).

This limited resolution prevented de novo chain tracing of the Cε1 domain for which there is no experimental structure. We therefore generated an alphafold2 model of the HMM5 Fab that as expected matches well our crystal structure of this Fab where the Cε1 domain was replaced by a Cγ1 domain (Plum, Tjerrild et al., 2022). This Fab model features the disulphide bridge pattern annotated in the uniprot entry IGHE_HUMAN (P01854) and is compatible with the presence of three Asn-linked glycans in the Cε1 domain (Fig. 2A). Due to the limited resolution, the location of the structurally homologous Cε1 and the CL domains could not be unambiguously derived directly from the 3D reconstruction, but comparison of the two possible orientations of the Fab model with the map strongly favored one of these orientations (Fig. 2B and supplementary Fig. 2B). In agreement with the selected orientation of the Cε1-CL domain tandem, there is excess density around especially Asn137 and Asn165 compatible with the above mentioned Asn-linked glycans in the Cε1 domain (supplementary Fig. 2C). This orientation was therefore selected for model building and refinement against the consensus map.

The deposited model fitting the consensus map (Table 1) contains the entire complex except for the variable domains of the Fab arms. The Fab elbow angle measures the angle between the two pseudo-dyad axes relating the two variable domains and the two constant domains, respectively (Stanfield, Zemla et al., 2006). In the crystal structure of the HMM5 where the Cε1 domain is replaced by a Cγ1 domain, the elbow angle is 136°. By measuring the correlation between the consensus 3D map and molecules in a library of 2468 known Fab structures, we found that the Fab structure in the protein data bank (pdb) entry 4dw2 with an elbow angle of 120° fitted the 3D map for both Fab arms better than any other structure in the library. Consequently, an optimized model of the full IgE bound to FcεRIα was created by superposition of the variable domains of the HMM5 structure onto the variable domains in the 4dw2 structures fitted at each Fab arm (Fig. 2C and

supplementary Fig. 2B). In the resulting model, the angle between the Fab arms is 167° and the separation of the two antigen binding sites is 18 nm. Both Fab arms are stably associated with their respective Cε2 domain in two distinct orientations that differ by 12° (Fig. 2D). The overall appearance of the IgE in the complex resembles that of a slightly distorted T, and if the C-terminal end of the FcεRIα ectodomain is perpendicular to the cell surface, the Fab arms and the Cε4 domain tandem will roughly be parallel to the membrane (Fig. 2C).

Since the distal Fab in this T conformation is far from the Cε3-4 domains, it must primarily be the hinge residues and the surrounding residues in the Cε1, CL and Cε2 domains that controls the spatial relationship between the Fab arms and the Cε2 domain tandem. At the proximal Fab, the linker connecting the VH and the Cε1 domains is close to His381 in the Cε3 domain of the same chain. At a low contour level in the consensus map, a density connecting these regions is visible (supplementary Fig. 2B). Such additional weak direct contacts formed between the proximal Fab and the Cε3 domain offer an explanation for the difference between the two Fab-hinge-Cε2 conformations. Without the putative Cε3 contact, the hinge conformation at the distal Fab is probably favored energetically over the hinge conformation at the proximal Fab.

The IgE Fc conformation in complex with FcεRI

Prior structures of the FcεRIα ectodomain in complex with the Cε3-4 and the Fc fragments of IgE revealed that the receptor binding site has contributions from both Cε3 domains and that IgE Fc adopts an asymmetric bent conformation with the Cε2 domain tandem placed oppositely of the FcεRI (Garman et al., 2000, Holdom et al., 2011). Comparison of our cryo-EM structure with the crystal structure of the IgE Fc-FcεRI complex demonstrates that the overall features of the receptor-Fc complex with the two interaction sites Cε3A and Cε3B are preserved in the receptor-IgE complex (Fig. 2E). The ε chain recognized by the FcεRIα Cε3A site contains the Cε1 domain of the distal Fab, whereas ε chain in the Cε3B site contains the Cε1 domain of the proximal Fab (Fig. 2C and 2E).

Structure of the IgE-FcεRI complex

An important descriptor for the overall conformation of the IgE Fc is the bending of the Cε2 domain tandem relative to the two-fold symmetry axis relating the two Cε3 and Cε4 domains. In the IgE containing cryo-EM structure, we measure an Fc bending of 107° that may be compared to 110° in the IgE Fc complex with the FcεRIα ectodomain (Holdom et al., 2011). When the two structures are superimposed on FcεRIα, the orientation of the Cε2 tandem differ by a coordinated 6° rotation relative to the FcεRIα (Fig. 2F). Based on the crystal structures of Ig Fc and its complex with FcεRIα, it was earlier reported that a β-strand shift occurred within the Cε2 domain between the two β-sheets upon complex formation with the receptor (Holdom et al., 2011). Our maps do not support such a strand shift (supplementary Fig. 2D), and the topology of Cε2 domain in our model of FcεRIα bound IgE is that observed in crystal structures of unbound IgE Fc (supplementary Fig. 2E) (Dore, Davies et al., 2017).

In addition to the bending of the Cε2 domain tandem, the Fc Cε3-4 sub-fragment can adopt multiple conformations ranging from closed to open depending on the spacing of their Cε3 domains and Cε3 distance to the Cε4 domains (Wurzburg & Jardetzky, 2009). This conformational flexibility allows the Cε3 domains to rotate ("swing") relative to each other. FcεRI and CD23 recognize different conformations of the IgE Cε3-4 domains, the open and closed state, respectively. In our cryo-EM structure, the Cε3-4 domains are in the open conformation as in the Fc-FcεRI crystal structure. A more detailed analysis of the Cε3-4 sub-fragment conformation reveals that the two Cε3 domains differ by 6° rotations compared to the Fc containing crystal structure while maintaining the distances between the N- and C-terminal ends of the two Cε3 domains (Fig. 2G). In summary, there are small but significant conformational changes within the Fc part in the cryo-EM structure of full IgE in complex with the FcεRIα ectodomain compared to the crystal structure of the complex containing only the Fc fragment. These differences are likely to be caused by the presence of the Fab arms in the cryo-EM structure, but lattice interactions may also have influenced the conformation of IgE Fc in the crystal structure (Holdom et al., 2011).

An alternative conformation of the receptor bound IgE conformation

During our efforts towards obtaining the cryo-EM structure of receptor bound IgE, we used negative stain (ns) EM to assess sample quality. We also obtained a single ns-EM 3D reconstruction of the HMM5 IgE-FcεRIα complex (Fig. 3A and supplementary Fig. 3). A model of the IgE Fc and the bound receptor ectodomain extracted from the cryo-EM structure was fitted easily in this 3D reconstruction, but no definite choice of the hand of the 3D reconstruction could be made by comparison of map-model correlation for the two possible hands of the map. There are well defined densities for both Fab arms in the ns-EM 3D reconstruction with the expected lower level of map intensity at the border between the variable and the constant domains (Fig. 3A) and the Fab arms are also clearly visible in the 2D classes (supplementary Fig. 3A). Hence, the ns-EM 3D reconstruction gives further support to the concept that in FcεRIα bound IgE, the Fab arms are fixed relative to the Fc like they are in unbound IgE (Jensen et al., 2020). However, the orientations of the Fab arms relative to the IgE Fc in the ns-EM 3D map are significantly different from those present in the cryo-EM structure, compare Figures 2C and 3A. In the ns-EM conformation, the antigen binding sites are separated by 13-14 nm and the angle between the Fab arms is ~73° as opposed to 18 nm and 167° in the cryo-EM model of FcεRI bound IgE. For simplicity, below we refer to these two conformations as Y (ns-EM) and T (cryo-EM), respectively. Only one ns-EM 2D class appears to contain IgE in the T conformation (supplementary Fig. 3A).

The observed significant difference in the two receptor bound conformation of IgE raised the question whether one of these conformations is an artefact arising from EM methodology. To address this concern, we conducted a synchrotron SEC-SAXS experiment in which the scattering from the IgE-FcεRIα complex eluting from a size exclusion column was continuously recorded. Data analysis suggested a complex in solution with a maximum extent of 17 nm (supplementary Fig. 4A-C). To enable a direct comparison between the two different EM conformations, we calculated scattering curves from molecular models fitted into the two 3D reconstructions. Both visually showed significant deviations from the observed scattering curve and χ^2 values of 28-44 for the fit

between the observed and the calculated scattering curves (supplementary Fig. 4D-E). We therefore asked whether the observed data could be described as a linear combination of these two calculated curves, which would mean that in solution a mixture of the conformations is present, but this did not result in a satisfactory description of the observed curve. We therefore also calculated scattering curves from dummy atom models derived directly from the two EM maps, and again both calculated curves were significantly different from the experimental curve (Fig. 3B). But a linear combination of these two calculated curves with 67% and 33% contribution from the cryo-EM and ns-EM curves, respectively, fitted the experimental SAXS curve in a reasonable manner with a χ^2=1.62 (Fig. 3C). This suggests that both conformations of the IgE-FcεRIα complex observed with EM occur in significant fractions under the solution conditions used for the SAXS experiment and that the content of other conformations may be minor. Interestingly, IgE in the Y conformation from the IgE-FcεRIα complex (Fig. 3A) could be docked as a single rigid body into our prior ns-EM 3D reconstruction of unbound HMM5 IgE (Jensen et al., 2020) with a correlation coefficient of 0.74 (Fig. 3D). This argues that ns-EM favors a similar conformation of IgE regardless of whether the antibody is bound to FcεRIα or not.

Increased Fab mobility lowers antigen stimulated IgE receptor activity

To understand why the IgE Fab-Fc hinge is rigid, we aligned available sequences of the epsilon heavy chain (Fig. 4A). The hinge residues Ser222-Pro227 connecting the Cε1 domain in the Fab to the Fc Cε2 domain in the IgE Fc are not highly conserved, but a constant feature is a nonpolar residue (F/V/I/L) at the position equivalent of Phe225 in our structure. The resolution of our 3D reconstruction prevents us from performing a detailed analysis of the role of Phe225 in the hinge, but it is clear that this residue experiences different surroundings at the two Fab-Fc hinges. At the proximal Fab, Phe225 appears to be close to Tyr313 in the connected Cε2 domain and not in the proximity of the light chain (Fig. 4B). At the distal Fab, Phe225 is close to Phe318 in the Cε2 domain and the C-terminal residues of the light chain including the light chain Cys217 engaged in a disulphide bond with Cys131 in the heavy chain (Fig. 4C). Notably, the presence of aromatic residues at positions 313 and 318 is rather well conserved and there appears to be co-evolution between the

linker region and the nearby residues 313-318 in the Cε2 domain (Fig. 4A). For the Y conformation of FcεRI bound IgE observed by negative stain we cannot define the linker conformation. But, as the overall locations of the two Fab arms are rather different in the T and Y conformations (Fig. 2 and Fig. 3), there could be up to four different conformations of the linker for FcεRI bound IgE that supports a stable Fab-Fc association.

The EM studies of FcεRIα bound IgE presented here and our prior study of free IgE and IgE in complex with ligelizumab (Jensen et al., 2020) provide convincing evidence that the Fab arms are associated with the nearby Cε2 domains in a limited number of stable conformations. In order to assess the biological impact of IgE rigidity in the context of its interplay with the receptors, we took advantage of the fact that the monoclonal HMM5 IgE exhibits reactivity to two similar carbohydrate structures, MUXF3 and MMXF3 differing by a mannosyl group (Fig. 5A), but with clearly different affinities (Plum et al., 2022). A flexible derivative of the HMM5 IgE was established by inserting a glycine-serine peptide linker between the Cε1 and Cε2 domains. This derivative termed HMM5L was expressed and purified like the HMM5 antibody in a similar yield (Fig. 5B-C). Notably, a minor difference in SDS-PAGE migration was observed (Fig. 5B-C). The flexibility of the derivative was verified by ns-EM (supplementary Fig. 5A), but the binding kinetics determined for the HMM5 and HMM5L interaction with immobilized FcεRIα ectodomain were very similar (supplementary Fig. 5B-E). Hence, the stable association of the Fab arms with the Fc does not contribute to affinity for the receptor FcεRI.

The potential of HMM5 IgE and its flexible derivative for activation and degranulation of effector cells by FcεRI cross-linking was assessed by measuring β-hexosaminidase release from RBL-SX38 cells, rat basophilic leukemia cells expressing the human FcεRI. Since receptor cross-linking by a monoclonal IgE like HMM5 demands the availability of more than one epitope per allergen we used horseradish peroxidase (HRP) carrying the MMXF glycan and a MUXF conjugate, consisting of bromelain-derived glycans coupled chemically to HSA, both of which display multiple cross-reactive

carbohydrate determinant (CCD) epitopes. Both HMM5 and HMM5L exhibited clear β-hexosaminidase release as marker for cellular activation for both antigens, although as expected at different concentrations (Fig. 5D). However, for the lowest concentrations of MMXF3 antigen, a noticeable reduction in cellular activation was observed for HMM5L compared to HMM5 suggesting that the introduction of the linker compromised the activity of IgE in this assay to some degree for the low affinity antigen MMXF3.

The low affinity IgE receptor CD23 is crucial for binding, uptake and presentation of allergens in form of allergen/IgE complexes and considered as another important driver of allergic immune responses. Therefore, our IgE variants were also evaluated for facilitated antigen binding (FAB) to CD23 using a surface-based variant of the FAB assay, the ELIFAB assay (Mobs, Muller et al., 2015). The HMM5 IgE and its flexible derivative HMM5L were used for formation of complexes with either the MUXF conjugate or HRP (Fig. 5E). These complexes bound efficiently to CD23, corroborating the general capability of the HMM5 IgE to form immune complexes of higher order and facilitate allergen binding via CD23. Notably, the binding of the immune complexes to CD23 was clearly diminished for the HMM5L IgE compared to the parental HMM5 IgE, again in particular for the lower affinity MMXF3 antigen from HRP. This reduction in IgE/antigen complex binding might be based on a varying complexation efficacy despite equivalent affinity or, alternatively, sterically different complex architectures resulting in a change in binding behavior. Taken together, data obtained with the two different functional assays suggest that rigidity of the Fab-Cε2 hinge, depending on the antigen and its architecture, is important for the biological function of IgE.

Hinge-less antibodies adopt distinct defined conformations

Like IgE, IgM have a short hinge between the Fab and the Fc and four constant domains Cμ1-Cμ4 in the heavy chain. In a recent cryo-EM structure of pentameric IgM, only one of the Cμ2 domain tandems were observed in a defined positions (Chen, Menon et al., 2022). With 3D variability analysis, it was possible to describe multiple related orientations of a structural unit consisting of

this Cμ2 tandem and the two associated Fab arms relative to the Cμ3-4 core. The angle between IgM Fab arms is ~28° and a similar angle was also observed in a tomography study of IgM in complex with complement component C1 (Sharp, Boyle et al., 2019). Likewise, a recent structure of B cell receptor IgM associated with the CD79αβ heterodimer features a similar orientation of the two Fab arms relative to the Cμ2 tandem(Dong, Pi et al., 2022). Hence, even though IgE and IgM both have short hinge regions and their Fab arms stably attached to the Cε2 and Cμ2 domains, respectively, the two distinct IgE conformations presented here are both clearly distinct from the Fab-Cμ2 arrangement observed in multiple structures of IgM (Fig. 6A). The IgY isotype found in birds and amphibians also features a heavy chain with four constant domains and lack of hinge. Evolutionary, IgM is the oldest antibody while IgE appears to have evolved from IgY (Zhang, Calvert et al., 2017). Negative stain EM studies of full IgY and a naturally occurring truncated variant of IgY lacking the last two domains of the heavy chain gave rise to two clear 2D classes for each IgY variant where the Fab arms and the Fc are can be clearly distinguished (Work, Dagenais et al., 2015). Hence, in IgY the Fab arms are stably attached with the Cu2 domain tandem as in IgE and IgM, but it is not clear whether one or two distinct IgY conformation were observed. It is therefore possible that IgY also adopt multiple stable distinct conformations.

The geometric properties of the two stable FcεRIα-bound IgE conformations we have identified in vitro with single particle in EM are summarized in Figure 6B. Importantly, our cryo-EM structure reveals an IgE molecule that is not that strongly bend but is flat with one Fab arm proximal to its own heavy chain. IgE is often depicted schematically as a quite bent molecule in order to align with classic fluorescence spectroscopy measurements that suggested a distance of 71 Å and 75 Å between the antigen-binding site and the C-terminus of the IgE heavy chain in FcεRI bound and fluid phase IgE, respectively (Zheng et al., 1992). In excellent agreement with this measurement, in the IgE T conformation from cryo-EM, there is 74 Å between IgE heavy chain Ser100 at the paratope of the proximal Fab and Ala542 at the C-terminal end of the same heavy chain. In contrast, in the Y conformation, the shortest equivalent distance is 91 Å (Fig. 6B).

Clearly, it is of strong interest to examine how these two IgE conformations may translate to the intact tetrameric membrane embedded FcεRIαβγ_2. Despite the lack of a detailed atomic structure of this receptor and the fact that we do not know exactly how the α-chain ectodomain is oriented spatially relative to the transmembrane part of the receptor, it appears that the T and Y conformations of the FcεRI bound IgE are likely to have different properties with respect to antigen recognition (Fig. 6C). If receptor bound IgE adopts the T conformation, the Fab arms and antigen binding site may be roughly parallel to the membrane. In contrast, if IgE adopts the Y conformation, the Fab arms are more likely to be pointing away from the membrane and capable of reaching towards antigens located further from the surface of the FcεRI presenting cell (Fig. 6C).

Discussion

Here we have provided firm structural evidence that IgE can adopt two distinct defined conformations when bound to the ectodomain of FcεRIα. We cannot exclude that the IgE conformation when bound to cellular FcεRI differs from that of the IgE-FcεRIα complex studied here, but since IgE is well separated from the membrane and the transmembrane parts of FcεRI, the two IgE conformations we observe are likely to represent *in vivo* relevant conformations. Fluorescence spectroscopy experiments suggested a distance of 71 Å and 75 Å between the antigen-binding site and the C-terminus of the IgE heavy chain in FcεRI bound and fluid phase unbound IgE, respectively (Zheng et al., 1992). In excellent agreement with this measurement, in the IgE T conformation from cryo-EM, this distance is 74 Å. This adds further support to the relevance of the T conformation and argues that a similar conformation occurs in unbound fluid phase IgE. For the ns-EM Y conformation, the equivalent distances are between 9-14 nm, much larger than the range of observed distances determined by fluorescence spectroscopy (Zheng et al., 1992). It should be noted that with this technique, distances beyond 10 nm are not well resolved. Nevertheless, the fluorescence measurements suggest that the Y conformation may be less abundant than the T conformation for IgE in complex with cell bound FcεRI. Accordingly, we estimate a 2:1 ratio between the two conformations in solution based on SAXS data for the IgE-FcεRIα complex. With respect to the

geometry of Fab arms, titration of an anti-DNP IgE with bivalent antigens suggested a separation of 13 nm between the two DNP paratopes(Schweitzer-Stenner, Licht et al., 1987) which is in excellent agreement with the 13 nm separation in the ns-EM Y conformation. In the T conformation, the distance is 17 nm, but divalent ligands capable of spanning this distance were not evaluated in (Schweitzer-Stenner et al., 1987), and consequently the T conformation if present could not be detected.

Since the IgE Fc and IgE bind FcεRIα with very similar affinity (Henry, Cook et al., 1997, Hight & Nadler, 1976) and also shown by us here (supplementary Fig. 5B-E), we do not expect significant differences in affinity for this receptor between the two IgE conformations. With respect to the second receptor CD23, the binding site is located in the Cε3 domain of IgE (Dhaliwal, Pang et al., 2017) , is distinct from the FcεRIα binding site, and requires the closed conformation within the Cε3-Cε4 part of IgE Fc. We notice that binding of CD23 binding to IgE appears to be incompatible with the IgE T conformation since the distal Fab is predicted to exert steric hindrance on CD23. It is therefore likely that the IgE T conformation is specific to the FcεRIα bound state and the unbound state. Further biophysical and ultrastructural characterization of IgE bound to FcεRI presenting cells is required to clarify the role of the two IgE conformations and how they may change in response to antigen binding and receptor crosslinking.

Super-resolution microscopy studies of (RBL)-2H3 mast cells showed that upon antigen stimulation the IgE-FcεRI receptor complexes form clusters that may reach a density of $4x10^3$ molecules/µm(Shelby et al., 2013) giving an average area of 25000 $Å^2$/molecule which is equivalent to a hexagon side length of 10 nm. With a maximum extent of 19 nm and 16 nm for the T- and Y-conformations, respectively, it is clear that regardless of the IgE conformation, such IgE-FcεRI receptor clusters induced by antigen crosslinking are quite densely packed in the plane of the membrane. Recent progress in cryo-electron tomography methodology (Turk & Baumeister, 2020) bears promise that a detailed structural understanding of such clusters of antigen cross-linked FcεRI

bound IgE are within reach and even has the potential to describe the conformations of individual IgE-FcεRI receptor complexes in these clusters. It will also be of particular interest to investigate whether either of the two conformations can associate or dissociate more easily with FcεRI or is dominating when antigens crosslink multiple receptors on a cell. The available data does not provide information about whether IgE can switch between the two conformations while bound to FceRI. If such a conformational change only occurs in unbound IgE, it may involve the two-fold symmetric transition state conformation of IgE Fc characterized by Sutton and coworkers (Drinkwater et al., 2014).

Our functional assays argue that structurally defined hinge conformations play a significant role in the biological activity of IgE. It is well described that different antibody isotypes exhibit varying capability to form complexes with the antigen in solution (Roux et al., 1998). Although the use of a monoclonal IgE simplifies the analysis in the functional assays performed in this study, the accompanying use of a polyvalent antigen for cellular activation and complex formation makes an extrapolation somewhat difficult. With more than 1000 allergens approved by the WHO/IUIS, individual target structures probably exhibit different susceptibility to rigid or flexible IgE molecules. Nevertheless, it appears reasonable that in the polyvalent setting of this study, an impact is primarily seen for a lower affinity interaction. Inversely, a high affinity interaction combined with increased avidity might be less amenable to reflecting the changes imposed by hinge flexibility in the biological activity of IgE. Similarly, allergens of different biochemical and three-dimensional nature and size might preferentially interact with the one or the other IgE conformation. Epitopes in direct proximity seem to establish more potent allergens, a concept which is supported by the fact that a large portion of allergens is actually rather small. Most studies however were based on single IgE antibodies with engineered or synthetic epitopes. In an allergic patient with the presence of an IgE repertoire of varying complexity, the impact of molecular rigidity, the conformational state and the consequences for the interaction with the two receptors could easily be profoundly stronger.

Author contributions

RKJ conducted all steps of the EM analyses and prepared the FcεRIα ectodomain. MM expressed and purified IgE and conducted the functional assays. RG performed all the experimental work related to SAXS data. EZ and GRA supervised research, analyzed data and wrote the paper together with RKJ, RG and MM.

Conflict of interest statement

The authors declare no competing interests.

Acknowledgements

GRA received research support from the Novo Nordisk Foundation, the Carlsberg Foundation, the Lundbeck Foundation, and the Danish Foundation for Independent Research (DFF). RKJ was supported by the DFF. ES received research support from the Novo Nordisk Foundation and the DFF. We are grateful to assistance with data collection and processing offered by the EMBL Hamburg staff at the P12 SAXS beamline. We acknowledge Diamond Light Source for access to and support of the cryo-EM facilities at the UK's national Electron Bio-imaging Centre (eBIC), and to Mirian Weckener and Dan Clare at eBIC for their assistance with preparing grids on the eBIC chameleon. We also thank the electron microscopy facility at Aarhus University for their assistance with data collection of negative stain EM and initial screening of cryo EM grid conditions.

Materials and Methods

Protein expression and purification.

Expression of HMM5 IgE was essentially performed as described previously (Bantleon, Wolf et al., 2016). Briefly, Sf9 cells were cultivated in HyClone Sfx-insect medium (Cytiva). Baculovirus production was performed by using the Bac-to-Bac system following the manufacturer's recommendations. HMM5 and HMM5L plasmids were transformed into DH10Bac™ *E.coli* and the recombinant bacmid DNA was isolated and transfected into SF9 cells using Cellfectin II (Thermo

Fisher Scientific). After two rounds of virus amplification, the appropriate virus concentration for expression was analyzed by infecting Sf9 cells with different amounts of virus and analyze protein expression by immunoblot 5 days after infection. For expression 500 ml Sf9 cells $1x10^6$ cells /ml were infected with virus and incubated under shaking for 5 days at 27°C.

To create the HMM5L variant with a flexible hinge, a 10 amino acid $(SG_4)_2$ linker was inserted between amino acid residues 223 and 224 of the HMM5 IgE. In order to insert the SG linker, a gene string (GenArt) containing the IgE-Fc sequence fused to the SG linker was ordered and cloned between *SalI* and the *BglII* of IgE-Fc. The IgE-FC linker was then inserted via *XhoI* and *HindIII* into pFastBac dual containing HMM5 kappa light chain and the heavy chain variable region (pFBM5hIgE). After expression, the antibodies were purified from the culture medium using a capture with a 5 ml HisTrap excel column (Cytiva). The column was washed with 20 column volumes (CVs) 20 mM NaPO4, 0.5 M NaCl, 30 mM imidazole, pH 7.4 and eluted with 15 CVs 20 mM NaPO4, 0.5 M NaCl, 500 mM imidazole pH 7.4. The concentrated eluate was further purified by size exclusion chromatography using on a HILoad 16/600 Superdex 200pg column (Cytiva) equilibrated in 20 mM HEPES, 50 mM NaCl pH 7.0. A final SEC chromatography step was performed on a 24 ml Superdex 200 increase (Cytiva) equilibrated in 20 mM HEPES pH 7.5, 150 mM NaCl.

For expression in HEK293 cells, the cells were incubated in DMEM high glucose L-glutamine (Sigma-Aldrich) supplemented with 10% fetal calf serum and 0.1 kIU/L penicillin and 0.1 mg/mL streptomycin. For transfection, $5x10^5$ cells per 6-well were seeded and 20 h later transfected with 4 µg of DNA using polyethylene imine (Polysciences) in a DNA:PEI ratio of 1:3. For stable expression, the cells were passaged in a ratio 1:5 3 days after transfection and exposed to zeocin (invivogen). After 2 weeks of selection, single colonies were isolated and protein expression was analyzed by immunoblot. For expression, cells of a confluent T175 flask were transferred to an 850 cm^2 rolling bottle with 500 ml DMEM medium and incubated rolling for 14 days.

Structure of the IgE-FcεRI complex

The ectodomain of the FcεRIα subunit (residues 26-205) was expressed in HEK293S cells transfected with PEI as described in (Pedersen, Jensen et al., 2020). The cell supernatant was collected after 4 days and applied to a 5 mL HisTrap Excel (Cytiva). The column was washed twice with 25 mL of 20 mM TRIS pH 8.0, 500 mM NaCl, and FcεRI was eluted in 20 mL of 20 mM TRIS pH 8.0, 250 mM Imidazole. The FcεRIα was added 1:100 (w:w) TEV protease and was dialyzed 2 hours against 2 L of 20 mM HEPES pH 7.5, 150 mM NaCl at room temperature followed by 16 hours at 4 °C against 2 L of 20 mM HEPES pH 7.5, 150 mM NaCl. The protein was applied to a 5 mL HisTrap HT, and FcεRIα was collected in the flow through of the column. The protein was concentrated using a vivaspin 6 (Merck) with a molecular weight cut off of 10 kDa, and thereafter applied to a 24 ml Superdex 200 increase (Cytiva) equilibrated in 20 mM HEPES pH 7.5, 150 mM NaCl. The IgE-FcεRIα complex was formed by mixing IgE with a two-fold molar excess of the receptor. The complex was incubated for at least 30 minutes on ice, before being applied to a 24ml Superdex 200 increase SEC column (Cytiva) equilibrated in 20 mM HEPES pH 7.5, 150 mM NaCl.

Mediator release assay.

RBL-SX38 cells were cultivated in a CO_2 incubator at 37°C with MEM, 15% heat-inactivated fetal calf serum with 0.1 kIU/L penicillin, 0.1 mg/mL streptomycin, 1 mM sodium pyruvate and 1 mg/mL G418 (Sigma-Aldrich). In vitro degranulation was analyzed as described previously (Plum et al., 2022) (Hecker, Diethers et al., 2011). One day prior to the assay, $1x10^5$ cells per 96 well were seeded. After sensitization with 100 ng of IgE in culture-medium for 2h, different concentrations of CCD-carrying proteins were added in Tyrode's buffer (10mM HEPES,13 mM NaCl, 5mM KCl, 1.4mM $CaCl_2$, 1.0 mM $MgCl_2$, pH 7.4, 5.6 mM glucose, 0.1% w/w BSA) and incubated for 60 min at 37 °C. As a reference, cross-linking was achieved by 100 ng polyclonal rabbit anti-human IgE antibody (Dako A0094). β-Hexosaminidase release of viable versus lysed cells was assessed with 8 mM p-nitrophenyl N-acetyl-glucosaminopyranoside in 0.1 M citrate buffer pH 4.5. The reaction was stopped with 0.1 M carbonate buffer pH 10 and the absorbance measured at 405 nm.

CD23 binding in the ELIFAB assay.

In order to analyze the immunocomplex formation and their binding to CD23, a surface-based ELIFAB assay was performed (Shamji, Francis et al., 2013). Immunocomplexes were formed by adding 20 µL HMM5 or HMM5L IgE (10 µg/ml in RPMI) to 20 µL RPMI and 5 µL antigen followed by incubation for 1h at 37°C. The preincubated immunocomplexes were transferred to overnight coated and BSA-blocked recombinant CD23 (625 ng/ 96 well in PBS (R&D systems 123-FE-050)). After washing; IgE antigen complexes bound to immobilized CD23 were detected by adding biotin-conjugated anti-human IgE antibody (0.5 µg/mL) (BD-Pharmingen Cat 55585) followed by detection with ExtrAvidin AP (Sigma E2636) and p-nitrophenyl phosphate 5 mg/mL (Sigma 4876) in alkaline phosphate buffer.

Bio-layer interferometry

All BLI experiments were performed on an Octet Red96 (Sartorius) at 30°C and shaking at 1000 rounds per minute using streptavidin biosensors (Sartorius). The experiments were performed in 20 mM HEPES pH 7.5, 150 mM NaCl, and regeneration was performed in three rounds of 30 seconds using 2 M NaCl, 100 mM Acetate pH 4.0. First FcεRIα was biotinylated O/N at 4°C in 20 mM HEPES pH 8.0, 150 mM NaCl, 10 mM ATP, 50 µM biotin, 10 mM $MgCl_2$ and BirA in 1:10,000 (w:w). BirA was removed by using a 24 ml Superdex 75 increase (Cytiva) SEC column. The streptavidin sensors were loaded with 5 µg/mL biotinylated FcεRIα for 2 minutes, and subsequently washed thrice with running buffer. Association was then measured to IgE Fc (12.5, 6.3, 3.1, 1.6, 0.78, 0.39 nM), HMM5 (25, 12.5, 6.3, 3.1, 1.6, 0.78, 0.39 nM) or HMM5L (50, 25, 12.5, 6.3, 3.1, 1.6, 0.78n nM) for 300 seconds, followed by a 300 seconds dissociation period. The association was modeled as $R(t)=R_{max}([IgE]/([IgE]+K_D)(1-\exp(-t(k_{on}[IgE]-k_{off})))$, $K_d=k_{on}/k_{off}$, and the dissociation was modelled as a first order exponential decay, $R(t) = R(300)\exp(-k_{off}(t-300\ s))$. The given values correspond to the average of three (HMM5 IgE, IgE Fc) or two (HMM5L IgE) experiments ± the standard deviation.

Cryo-EM grid preparation, data collection and processing.

The purified IgE-FcεRIα complex was concentrated to 3.2 mg/mL, and applied to Quantifoil Active grids (SPT Labtech) using the Chameleon (SPT Labtech) at the United Kingdom national electron Bio-Imaging Centre (eBIC). Micrographs were collected on a 300 kV Titan Krios microscope (ThermoFischer) at eBIC, equipped with a Bio-quantum-K3 detector and an energy filter (Gatan). For data collection spot size 5 and a C2 aperture of 70 µm were used, while micrographs were collected with EPU using at 105k x magnification, and a physical pixel size of 0.829 Å. The data were collected in super resolution mode with an assumed defocus of -1.8 µm to -0.8 µm, varied in 0.2 µm steps. Each micrograph was collected with a dose of 59.16 $e^-/Å^2$ divided over 40 frames. Raw super-resolution movie frames were imported into CryoSparc v3 (Structura Biotechnology 33 Inc) (Punjani, Rubinstein et al., 2017). The movies were initially aligned using patch motion correction with a maximum alignment resolution of 5 Å, B factor blurring of 500 Å, and cropping the output two-fold to the physical pixel size. The CTF was estimated using patch CTF estimation with default parameters. Movies with defocus outside of 0.5 µm and 4 µm were removed, corresponding to 204 movies. Particles were picked using the blob picker giving a total of 2,936,131 particles which were extracted with 5-fold binned data. Iterative rounds of 2D classification yielded a dataset corresponding to 634,649 particles. The particles were cleaned with a round of ab initio model generation using three classes. The two best classes were refined using 3D heterogeneous refinement with three classes. The best two classes from heterogeneous refinement, corresponding to 573,328 particles were re-extracted at 2-fold binning and a consensus model was refined. The consensus model was subsequently refined using non-uniform refinement (Punjani, Zhang et al., 2020). The refined model was used to perform local motion correction, followed by a new round of non-uniform refinement. The resulting angles were used to perform focused refinement on the FcεRI and IgE Cε2-4 to obtain well refined angles for the least flexible part of the structure. Subsequently, we performed local CTF alignment, and a final round of non-uniform refinement giving corresponding to the final cryo EM map of the full IgE at a global resolution of 4.1 Å. A final

round of focused refinement on FcεRI and IgE Cε2-4 gave the final 3D reconstruction for focused refinement with a resolution of 3.8 Å.

Structure refinement and analysis

Chimera-X (Pettersen, Goddard et al., 2021) was used for map inspection and initial fitting of models to 3D reconstructions. A model of the Fab containing the Cε1 domain was prepared with alphafold2 (Tunyasuvunakool, Adler et al., 2021). Programs from the PHENIX package (Liebschner, Afonine et al., 2019) version 1.19 or 1.20 was used for real space refinement, analysis and validation of cryo-EM structures. The graphics program COOT (Emsley, Lohkamp et al., 2010) was used for manual rebuilding of models prior to real space refinement in PHENIX. All figures presenting atomic models and 3D reconstructions were prepared with PYMOL, https://pymol.org/pymol.html or Chimera-X. To establish the optimal conformation of the two Fab moieties, models in a library containing 2468 unique Fab structures was superimposed onto the constant domain in the two light chains of an initial model refined against the consensus map. The correlation between the two fitted Fab molecules and the map was calculated with Chimera-X. The Fab in pdb entry 4dw2 was found to have the highest correlation for both Fab arms. An optimal model for the full IgE was next constructed by superposition of the variable domains from the structure of the HMM5 Fab in pdb entry 5i8o onto the variable domains of the two models of 4dw2 fitted to the two Fab arms in the model of the IgE-FcεRIα complex.

Negative stain EM

Carbon-evaporated copper grids (G400-C3, Gilder), were glow-discharged at 25 mA for 45 seconds using an easiGlow instrument (PELCO). The IgE-FcεRIα complex were blotted on the grids at 10 µg/mL and incubated for 5 seconds. The grid was then washed in 3 µL deionized water twice, followed by a 45 second incubation with 5 µL Nano-W (Nanoprobes). The stain was plotted away and the grids were air-dried before being imaged on a 120 kV Tecnai G2 spirit electron microscope. Automated data collection was performed using the program leginon (Cheng, Negro et al., 2021) , at

a nominal magnification of 67,000x and a defocus range of -0.4 to -1.7 µm. Particles were picked in cisTEM (Grant, Rohou et al., 2018), and 2D classification, initial model generation, and 3D refinement was performed in RELION-3 (Zivanov, Nakane et al., 2018).

SAXS analysis

SEC-SAXS measurements were performed on the IgE-FcεRIα complex at P12 beamline at Petra III, DESY (Hamburg, Germany). The HMM5 IgE and the purified FcεRIα ectodomain were dialyzed against 2 L of 25 mM HEPES pH 7.5, 150 mM NaCl for 24 h at 4°C and concentrated to 5.5 mg/ml. To reconstitute the IgE-FcεRIα complex, IgE was mixed with a two-fold molar excess of FcεRIα. The protein solutions were centrifuged at 15000 rpm for 15 min at 4°C prior to injection onto a Superdex 200 Increase 5/150 column (Cytiva) equilibrated in 25 mM HEPES pH 7.5, 150 mM NaCl for the in-line SEC-SAXS measurements. Programs in the ATSAS package version 3.0.3 or 3.0.5 (Manalastas-Cantos, Konarev et al., 2021) were used for data analysis using experimental data with a maximum q value of 0.2 $Å^{-1}$. Data analysis and reduction was performed with CHROMIXS and PRIMUS. Calculation of scattering profiles from the negative stain and cryo-EM EM 3D reconstructions was obtained by calculating dummy atom models with EM2DAM. For each map, three values of contour thresholds in EM2DAM for identification of dummy atoms were evaluated. Form factor calculation from dummy atom models was conducted with FFMAKER. The nine combinations of scattering curves were scaled in PRIMUS. Linear combination of two calculated curves to describe the experimental scattering curve was done with the OLIGOMER program. All plots of SAXS data were generated with PRIMUS.

Figure legends

Figure 1. Cryo-EM structure determination of the IgE-FcεRIα complex. A) Representation of the interplay and functional effects of IgE bound to its receptors FcεRI on basophils and mast cells (left) and CD23 on antigen presenting cells (right). B) Schematic outline of the IgE molecule with domain names. The IgE Fc moiety is formed by the Cε2-Cε4 domains in the two heavy chains (green and

blue), whereas the Fab is formed by the heavy chain domains VH and Cε1 together with the light chain (light blue and light green) VL and CL domains. The Fc moiety can interconvert between a symmetric straight conformation (top) and a bent conformation (bottom). C) Two orientations of the consensus cryo EM map of the IgE-FcεRIα complex contoured at 16 σ. Density around the receptor and the IgE Fc is grey and pink, respectively, whereas density at around the distal Fab (dFab) is green and density around the proximal Fab (pFab) is blue . D) As in panel C, but displaying a local resolution filtered map contoured at 6 σ to provide a better impression of the Fab arms. At the proximal Fab, the cleft between the variable the constant domains are visible. E) Map from the focused refinement centered on IgE-Fc and FcεRIα contoured at 20 σ. F-I) Examples of map quality from the focused refinement in Cε2 (F), Cε3 (G), Cε4 (H), and FcεRIα (I). The map is contoured at 12σ. In panels F-H, carbon atoms in one IgE heavy chain are colored blue, while carbons in the other heavy chain are green. In panel I, carbon atoms in the receptor α-subunit are colored grey, notice the clear density for the glycan linked to Asn42.

Figure 2. Cryo-EM reveals an IgE T conformation in complex with FcεRIα. A) Predicted alphafold2 model of the HMM5 IgE Fab with a Cε1 domain. Orange spheres mark three asparagines with N-linked glycans (top). Notice the location of the Cε1 specific disulfide bridge Cys131-221 next to the inter-subunit disulfide C130-C217CL (bottom). B) Superposition of the HMM5 crystal structure in the two possible orientations favors option 1 for distinguishing Cε1 and CL. C) The final structure of the IgE-FcεRIα complex. The Fab VL and VH domains are shown as cartoon as they are not present in the deposited structure due to low resolution of the 3D reconstruction at the variable domains in both Fab arms. D) Comparison of the two hinge regions and their connected Cε1-CL domain tandems. The two ε-chains are superimposed on their Cε2 domains. E) Details of the interaction between the receptor and the two Cε3 domains. Left, the Cε3A site interacting with an aromatic cluster in the FcεRI α1 domain. IgE Asp359 and Arg331 appear to engage in specific polar interactions with the receptor. Right, the at the Cε3B subsite, IgE Pro423 is inserted in a nonpolar pocket defined by three tryptophan side chains from FcεRIα while IgE Arg424 appears to engage in polar interactions. F) A

superposition of the Fc-FcεRIα and IgE-FcεRIα structures on the receptor reveals a difference in the location of the Cε2 tandem, possibly in response to presence of the Fab arms. G) Close-up after superposition on the receptor demonstrating a significant difference in rotation of the Cε3 domains between the Fc-FcεRIα and IgE-FcεRIα structures.

Figure 3. FcεRI bound IgE adopt the Y conformation in negative stain EM. A) At the top, a cartoon model of the IgE-FcεRIα complex is shown docked into the low resolution ns-EM 3D reconstruction (grey envelope). Below is displayed a surface model of the complex. Notice that the Fab heavy and light chains cannot be distinguished in this n-EM map. B) The experimental SEC-SAXS curve compared to the two curves predicted from the cryo-EM and the ns-EM 3D reconstructions, respectively. C) A linear combination of the two predicted curves obtained with the OLIGOMER program fits the data with χ^2=1.62. D) Docking of IgE from the FcεRIα in panel A as a single rigid body into the negative stain EM 3D reconstruction obtained with IgE itself. The map-model correlation of 0.74 suggests that unbound IgE can adopt a conformation close to the Y conformation of FcεRIα bound IgE.

Figure 4. The conformations of the hinge regions are different. A) Conservation of the hinge and the hinge contact region in the Cε2 domain. B) Close-up on the hinge at the proximal Fab with Phe225 in contact with the Cε2B domain. C) At the distal Fab, the hinge regions is sandwiched between the Cε2A domain and the C-terminal end of the CL domain.

Figure 5. Introduction of flexibility in the hinge may alter the interaction of IgE with both its receptors. A) Schematic drawing of the two glycans recognized by the HMM5 IgE. The lower affinity antigen MMXF3 is found on HRP, the higher affinity antigen MUXF3 on pineapple stem bromelain. B) SDS-PAGE analysis of HMM5 IgE and HMM5L IgE under non-reducing and reducing conditions after size exclusion chromatography. The band around 170 kDa represents the fully assembled antibody, whereas the band at 60 kDa under reducing corresponds to the ε-chain. The light chains are not visible under these conditions. C) The identity of IgE was further confirmed by immunoblot using an

anti-human IgE antibody labeled with alkaline phosphatase for detection. D) Binding and cross-linking of the high-affinity receptor FcεRI was assessed by detection of β-hexosaminidase release from RBL-S38X cells upon passive loading with IgE followed by exposure to the antigens. Both IgE variants elicit β-hexosaminidase release, but HMM5L is less active with the lower affinity MMXF3 antigen. E) The ability of IgE to form immune complexes and the subsequent binding to immobilized CD23 was analyzed in ELIFAB assays. A clear reduction of complex binding to CD23 for HMM5L compared to HMM5, in particular for the lower affinity antigen, suggests a more efficient complexation or sterically different complex architecture.

Figure 6. The two IgE conformation are unique and may behave different in antigen recognition. A) Comparison of two Fab conformations of IgE with one of multiple similar Fab conformations from IgM (Chen et al., 2022). The two IgE Fab-Cε2 conformations are clearly distinct from the IgM Fab-Cμ2 conformation. B) Comparison of the IgE T and Y conformations of receptor bound IgE. Key distances (given in nm) measured between Ser100 and Ala542 in the two heavy chains and the Ser100-Ser100 distance between two Fabs are outlined. C) Models of IgE on cell bound FcεRI illustrates that the antigen binding paratopes of IgE in the Y-conformation (right) are likely to extend 50-75 Å further out from the cell surface compared to IgE in the T-conformation (left). The three vertically aligned dots in the center are placed 50, 100 and 150 Å above the surface.

Table 1. Statistics for cryo-EM data collection, refinement and validation. The lower part of the table was prepared with pheinx.validation_cryoem.

Data collection			
Microscope	FEI Titan Krios	No. of frames	40
Magnification	105,000	Defocus range (μm)	0.8-1.8
Voltage (kV)	300	Pixel size (Å)	0.829
Electron exposure ($e^-/Å^2$)	59.16	Symmetry imposed	C1
		No. of micrographs	11015

Deposited data	**Focused**	**Consensus**
PDB/EMDB entry	8C1B/ EMD-16377	8C1C/EMD-16378
Atoms	12675 (Hydrogens: 6106)	19267 (Hydrogens: 9284)
Residues	Protein: 807	Protein: 1237
Bonds (RMSD)		
Length (Å) (# > 4sigma)	0.007 (0)	0.007 (0)
Angles (°) (# > 4sigma)	1.257 (16)	1.156 (14)
MolProbity score	1.42	1.23
Clash score	3.18	2.40
Ramachandran plot (%)		
Outliers/ Allowed/ Favored	0.25/4.24/95.51	0.16/3.18/96.66
Rotamer outliers (%)	0.28	0.00
ADP (B-factors)		
Iso/Aniso (#)	6569/0	9983/0
min/max/mean		
Protein	74.57/252.79/131.77	33.87/999.99/346.65
Ligand	77.58/204.62/119.18	114.39/256.02/176.60
Data		
Box Lengths (Å)	96.37, 122.28, 103.62	116.06, 122.28, 138.86
Supplied Resolution (Å)	3.8	4.1
Resolution Estimates (Å)	Masked Unmasked	Masked Unmasked
d FSC (half maps; 0.143)	3.8 3.9	4.2 4.2
d model	3.9 4.0	4.0 4.1
d FSC model (0/0.143/0.5)	3.6/3.8/4.5 3.7/3.9/6.9	3.9/4.1/6.3 4.0/4.2/7.1
Map min/max/mean	-3.87/5.25/0.17	-1.18/3.26/0.13
Model vs. Data		
CC (mask)	0.70	0.71
CC (box)	0.76	0.87
CC (peaks)	0.53	0.66
CC (volume)	0.70	0.70
Mean CC for ligands	0.74	0.71

References

Bantleon F, Wolf S, Seismann H, Dam S, Lorentzen A, Miehe M, Jabs F, Jakob T, Plum M, Spillner E (2016) Human IgE is efficiently produced in glycosylated and biologically active form in lepidopteran cells. Mol Immunol 72: 49-56

Broide DH, Finkelman F, Bochner BS, Rothenberg ME (2011) Advances in mechanisms of asthma, allergy, and immunology in 2010. J Allergy Clin Immunol 127: 689-95

Burton DR (1990) Antibody: the flexible adaptor molecule. Trends Biochem Sci 15: 64-9

Chen Q, Menon R, Calder LJ, Tolar P, Rosenthal PB (2022) Cryomicroscopy reveals the structural basis for a flexible hinge motion in the immunoglobulin M pentamer. Nat Commun 13: 6314

Cheng A, Negro C, Bruhn JF, Rice WJ, Dallakyan S, Eng ET, Waterman DG, Potter CS, Carragher B (2021) Leginon: New features and applications. Protein Sci 30: 136-150

Clement MJ, Fortune A, Phalipon A, Marcel-Peyre V, Simenel C, Imberty A, Delepierre M, Mulard LA (2006) Toward a better understanding of the basis of the molecular mimicry of polysaccharide antigens by peptides: the example of Shigella flexneri 5a. J Biol Chem 281: 2317-32

Darrow MC, Moore JP, Walker RJ, Doering K, Thaw P, King RS (2019) chameleon: Next Generation Sample Preparation for CryoEM based on Spotiton. Acta Crystallogr A 75: A424-A424

Dhaliwal B, Pang MO, Keeble AH, James LK, Gould HJ, McDonnell JM, Sutton BJ, Beavil AJ (2017) IgE binds asymmetrically to its B cell receptor CD23. Sci Rep 7: 45533

Dong Y, Pi X, Bartels-Burgahn F, Saltukoglu D, Liang Z, Yang J, Alt FW, Reth M, Wu H (2022) Structural principles of B cell antigen receptor assembly. Nature 612: 156-161

Dore KA, Davies AM, Drinkwater N, Beavil AJ, McDonnell JM, Sutton BJ (2017) Thermal sensitivity and flexibility of the Cepsilon3 domains in immunoglobulin E. Biochim Biophys Acta Proteins Proteom 1865: 1336-1347

Drinkwater N, Cossins B, Keeble AH, Wright M, Cain K, Hailu H, Oxbrow A, Delgado J, Shuttleworth LK, Kao MW, McDonnell JM, Beavil AJ, Henry AJ, Sutton BJ (2014) Human immunoglobulin E flexes between acutely bent and extended conformations. Nat Struct Mol Biol 21: 397-404

Emsley P, Lohkamp B, Scott WG, Cowtan K (2010) Features and development of Coot. Acta Crystallogr D Biol Crystallogr 66: 486-501

Galli SJ, Tsai M (2012) IgE and mast cells in allergic disease. Nat Med 18: 693-704

Garman SC, Wurzburg BA, Tarchevskaya SS, Kinet JP, Jardetzky TS (2000) Structure of the Fc fragment of human IgE bound to its high-affinity receptor Fc epsilonRI alpha. Nature 406: 259-66

Glaeser RM (2018) Proteins, Interfaces, and Cryo-Em Grids. Curr Opin Colloid Interface Sci 34: 1-8

Gould HJ, Sutton BJ (2008) IgE in allergy and asthma today. Nature reviews Immunology 8: 205-17

Gould HJ, Sutton BJ, Beavil AJ, Beavil RL, McCloskey N, Coker HA, Fear D, Smurthwaite L (2003) The biology of IGE and the basis of allergic disease. Annual review of immunology 21: 579-628

Grant T, Rohou A, Grigorieff N (2018) cisTEM, user-friendly software for single-particle image processing. Elife 7

Hecker J, Diethers A, Etzold S, Seismann H, Michel Y, Plum M, Bredehorst R, Blank S, Braren I, Spillner E (2011) Generation and epitope analysis of human monoclonal antibody isotypes with specificity for the Timothy grass major allergen Phl p 5a. Mol Immunol 48: 1236-44

Henry AJ, Cook JP, McDonnell JM, Mackay GA, Shi J, Sutton BJ, Gould HJ (1997) Participation of the N-terminal region of Cepsilon3 in the binding of human IgE to its high-affinity receptor FcepsilonRI. Biochemistry 36: 15568-78

Hight ME, Nadler CF (1976) Relationships between wild sheep and goats and the aoudad (Caprini) studied by immunodiffusion. Comp Biochem Physiol B 54: 265-9

Holdom MD, Davies AM, Nettleship JE, Bagby SC, Dhaliwal B, Girardi E, Hunt J, Gould HJ, Beavil AJ, McDonnell JM, Owens RJ, Sutton BJ (2011) Conformational changes in IgE contribute to its uniquely slow dissociation rate from receptor FcvarepsilonRI. Nat Struct Mol Biol 18: 571-6

Hunt J, Keeble AH, Dale RE, Corbett MK, Beavil RL, Levitt J, Swann MJ, Suhling K, Ameer-Beg S, Sutton BJ, Beavil AJ (2012) A fluorescent biosensor reveals conformational changes in human immunoglobulin E Fc: implications for mechanisms of receptor binding, inhibition, and allergen recognition. J Biol Chem 287: 17459-70

Jensen RK, Jabs F, Miehe M, Molgaard B, Pfutzner W, Mobs C, Spillner E, Andersen GR (2020) Structure of intact IgE and the mechanism of ligelizumab revealed by electron microscopy. Allergy

Kraft S, Kinet JP (2007) New developments in FcepsilonRI regulation, function and inhibition. Nature reviews Immunology 7: 365-78

Liebschner D, Afonine PV, Baker ML, Bunkoczi G, Chen VB, Croll TI, Hintze B, Hung LW, Jain S, McCoy AJ, Moriarty NW, Oeffner RD, Poon BK, Prisant MG, Read RJ, Richardson JS, Richardson DC, Sammito MD, Sobolev OV, Stockwell DH et al. (2019) Macromolecular structure determination using X-rays, neutrons and electrons: recent developments in Phenix. Acta Crystallogr D Struct Biol 75: 861-877

Manalastas-Cantos K, Konarev PV, Hajizadeh NR, Kikhney AG, Petoukhov MV, Molodenskiy DS, Panjkovich A, Mertens HDT, Gruzinov A, Borges C, Jeffries CM, Svergun DI, Franke D (2021) ATSAS 3.0: expanded functionality and new tools for small-angle scattering data analysis. J Appl Crystallogr 54: 343-355

Mobs C, Muller J, Rudzio A, Pickert J, Blank S, Jakob T, Spillner E, Pfutzner W (2015) Decline of Ves v 5-specific blocking capacity in wasp venom-allergic patients after stopping allergen immunotherapy. Allergy 70: 715-9

Pedersen H, Jensen RK, Jensen JMB, Fox R, Pedersen DV, Olesen HG, Hansen AG, Christiansen D, Mazarakis SMM, Lojek N, Hansen P, Gadeberg TAF, Zarantonello A, Laursen NS, Mollnes TE, Johnson

MB, Stevens B, Thiel S, Andersen GR (2020) A Complement C3-Specific Nanobody for Modulation of the Alternative Cascade Identifies the C-Terminal Domain of C3b as Functional in C5 Convertase Activity. J Immunol 205: 2287-2300

Pettersen EF, Goddard TD, Huang CC, Meng EC, Couch GS, Croll TI, Morris JH, Ferrin TE (2021) UCSF ChimeraX: Structure visualization for researchers, educators, and developers. Protein Sci 30: 70-82

Plum M, Tjerrild L, Raiber T, Bantleon F, Bantleon S, Miehe M, Jabs F, Seismann H, Mobs C, Pfutzner W, Jakob T, Andersen GR, Spillner E (2022) Structural and functional analyses of antibodies specific for modified core N-glycans suggest a role in TH 2 responses. Allergy

Punjani A, Rubinstein JL, Fleet DJ, Brubaker MA (2017) cryoSPARC: algorithms for rapid unsupervised cryo-EM structure determination. Nat Methods 14: 290-296

Punjani A, Zhang H, Fleet DJ (2020) Non-uniform refinement: adaptive regularization improves single-particle cryo-EM reconstruction. Nat Methods 17: 1214-1221

Roux KH, Strelets L, Brekke OH, Sandlie I, Michaelsen TE (1998) Comparisons of the ability of human IgG3 hinge mutants, IgM, IgE, and IgA2, to form small immune complexes: a role for flexibility and geometry. J Immunol 161: 4083-90

Schweitzer-Stenner R, Licht A, Luscher I, Pecht I (1987) Oligomerization and ring closure of immunoglobulin E class antibodies by divalent haptens. Biochemistry 26: 3602-12

Shamji MH, Francis JN, Wurtzen PA, Lund K, Durham SR, Till SJ (2013) Cell-free detection of allergen-IgE cross-linking with immobilized phase CD23: inhibition by blocking antibody responses after immunotherapy. J Allergy Clin Immunol 132: 1003-5 e1-4

Sharp TH, Boyle AL, Diebolder CA, Kros A, Koster AJ, Gros P (2019) Insights into IgM-mediated complement activation based on in situ structures of IgM-C1-C4b. Proc Natl Acad Sci U S A 116: 11900-11905

Shelby SA, Holowka D, Baird B, Veatch SL (2013) Distinct stages of stimulated FcepsilonRI receptor clustering and immobilization are identified through superresolution imaging. Biophys J 105: 2343-54

Stanfield RL, Zemla A, Wilson IA, Rupp B (2006) Antibody elbow angles are influenced by their light chain class. J Mol Biol 357: 1566-74

Sutton BJ, Davies AM (2015) Structure and dynamics of IgE-receptor interactions: FcepsilonRI and CD23/FcepsilonRII. Immunol Rev 268: 222-35

Tunyasuvunakool K, Adler J, Wu Z, Green T, Zielinski M, Zidek A, Bridgland A, Cowie A, Meyer C, Laydon A, Velankar S, Kleywegt GJ, Bateman A, Evans R, Pritzel A, Figurnov M, Ronneberger O, Bates R, Kohl SAA, Potapenko A et al. (2021) Highly accurate protein structure prediction for the human proteome. Nature 596: 590-596

Turk M, Baumeister W (2020) The promise and the challenges of cryo-electron tomography. FEBS Lett 594: 3243-3261

Uzgiris EE (1987) Self-organization of IgE immunoglobulins on phospholipid films. Biochem J 242: 293-6

Work TM, Dagenais J, Breeden R, Schneemann A, Sung J, Hew B, Balazs GH, Berestecky JM (2015) Green Turtles (Chelonia mydas) Have Novel Asymmetrical Antibodies. J Immunol 195: 5452-60

Wurzburg BA, Jardetzky TS (2009) Conformational flexibility in immunoglobulin E-Fc 3-4 revealed in multiple crystal forms. J Mol Biol 393: 176-90

Zhang X, Calvert RA, Sutton BJ, Dore KA (2017) IgY: a key isotype in antibody evolution. Biol Rev Camb Philos Soc 92: 2144-2156

Zheng Y, Shopes B, Holowka D, Baird B (1992) Dynamic conformations compared for IgE and IgG1 in solution and bound to receptors. Biochemistry 31: 7446-56

Zivanov J, Nakane T, Forsberg BO, Kimanius D, Hagen WJ, Lindahl E, Scheres SH (2018) New tools for automated high-resolution cryo-EM structure determination in RELION-3. Elife 7

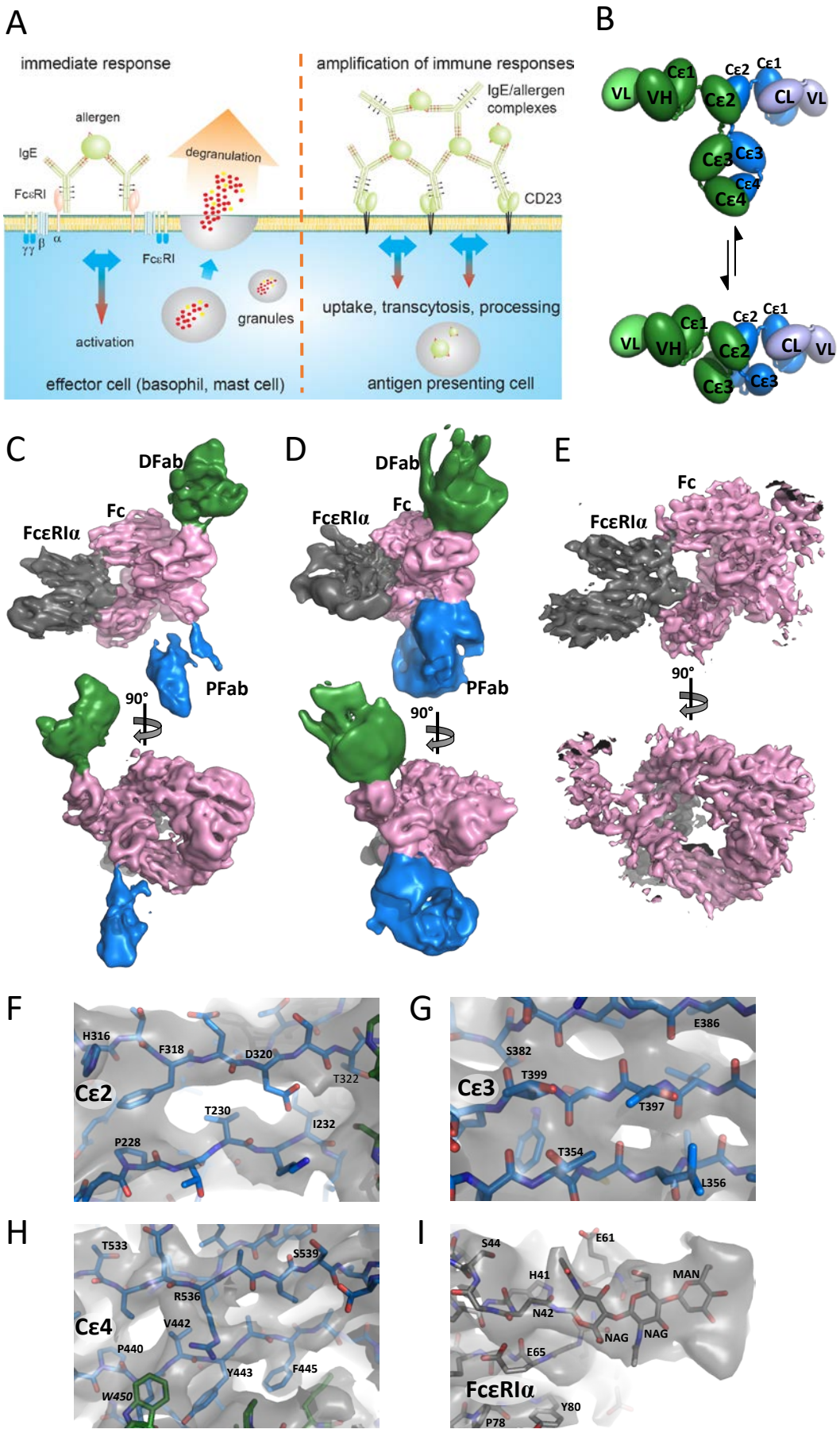
A
immediate response
amplification of immune responses
allergen
IgE
FcεRI
degranulation
IgE/allergen complexes
CD23
γγ β α
FcεRI
granules
activation
uptake, transcytosis, processing
effector cell (basophil, mast cell)
antigen presenting cell
B
VL
VH
Cε1
Cε2
Cε1
CL
VL
Cε2
Cε3
Cε3
Cε4
Cε4
VL
VH
Cε1
Cε2
Cε1
CL
VL
Cε2
Cε3
Cε3
C
DFab
Fc
FcεRIα
PFab
90°
D
DFab
Fc
FcεRIα
PFab
90°
E
Fc
FcεRIα
90°
F
H316
F318
D320
T322
Cε2
T230
I232
P228
G
E386
S382
T399
Cε3
T397
T354
L356
H
T533
S539
R536
Cε4
V442
P440
Y443
F445
W450
I
S44
E61
H41
MAN
N42
NAG
NAG
E65
FcεRIα
Y80
P78

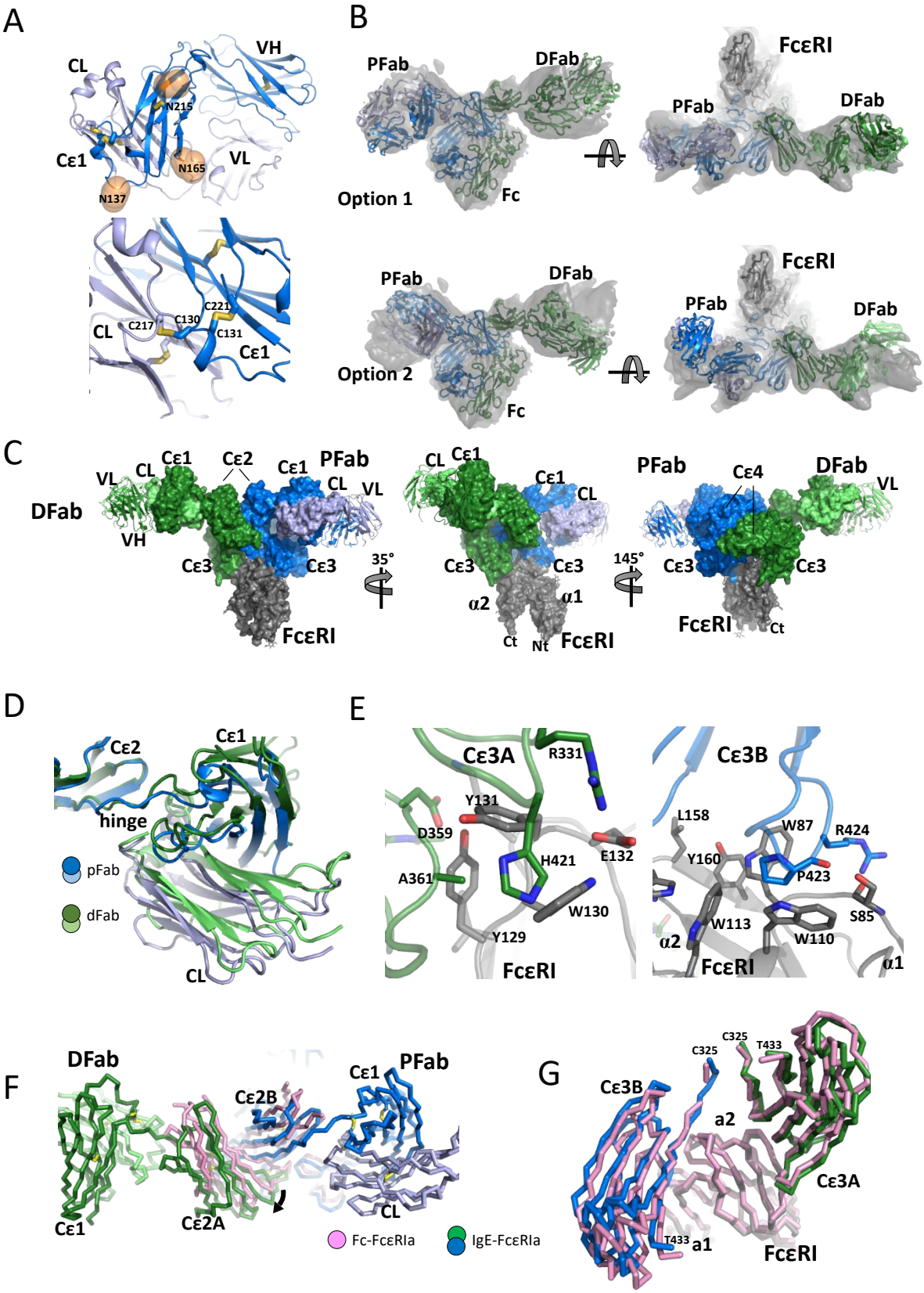
A
CL
VH
N215
Cε1
N165
VL
N137
C221
C217
C130
C131
CL
Cε1
B
PFab
DFab
FcεRI
PFab
DFab
Option 1
Fc
PFab
DFab
FcεRI
PFab
DFab
Option 2
Fc
C
VL
CL
Cε1
Cε2
Cε1
PFab
CL
VL
DFab
VH
Cε3
Cε3
FcεRI
35°
CL
Cε1
Cε1
CL
Cε3
Cε3
α2
α1
Ct
Nt
FcεRI
145°
PFab
Cε4
DFab
VL
Cε3
Cε3
FcεRI
Ct
D
Cε2
Cε1
hinge
pFab
dFab
CL
E
Cε3A
R331
Y131
D359
E132
H421
A361
W130
Y129
FcεRI
Cε3B
L158
W87
R424
Y160
P423
S85
W113
W110
α2
FcεRI
α1
F
DFab
Cε1
PFab
Cε2B
Cε1
Cε2A
CL
Fc-FcεRIa
IgE-FcεRIa
G
C325
C325
T433
Cε3B
a2
Cε3A
T433
a1
FcεRI

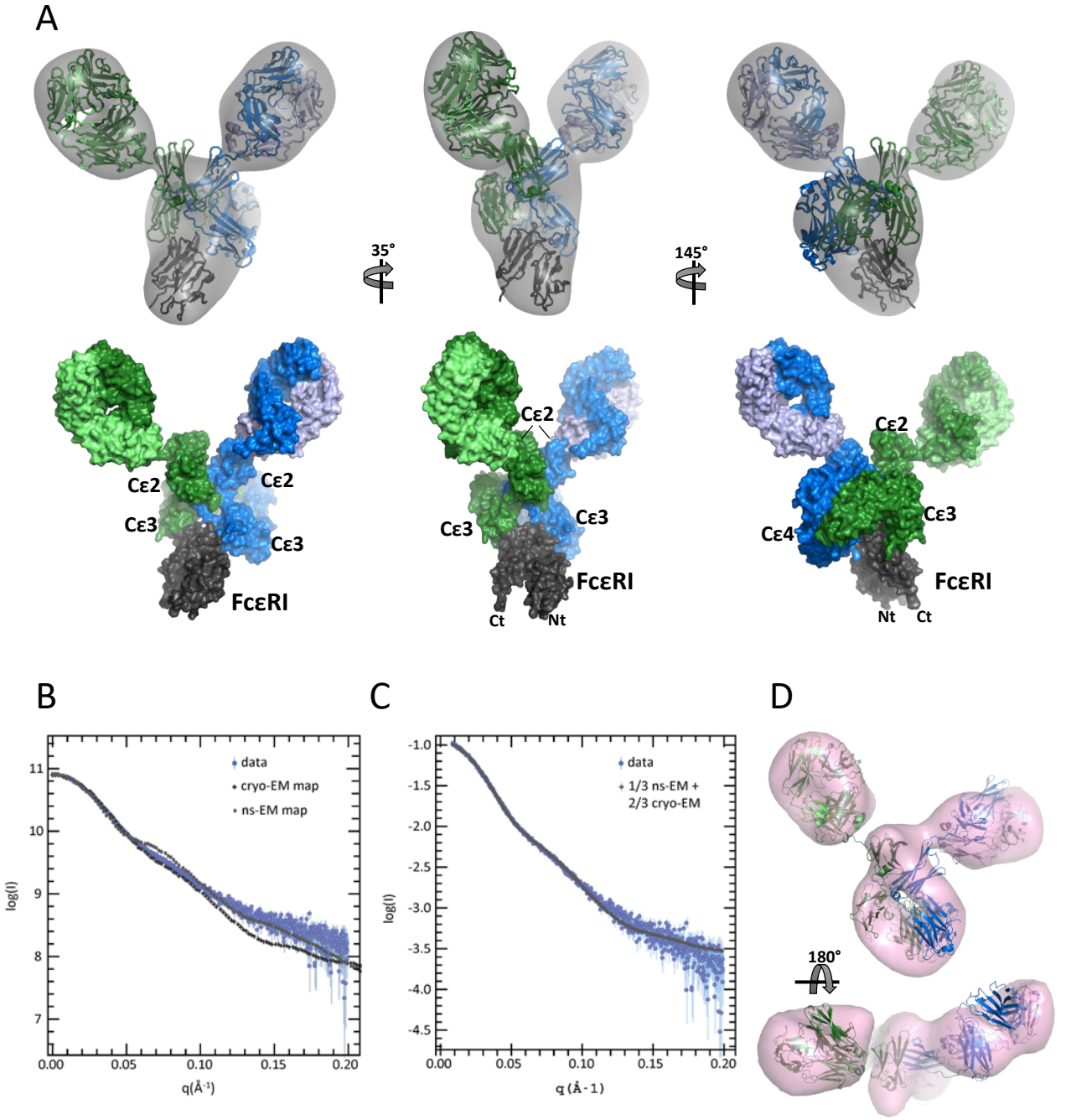
A
35°
145°
Cε2
Cε2
Cε3
Cε3
FcεRI
Cε2
Cε3
Cε3
FcεRI
Ct
Nt
Cε2
Cε3
Cε4
FcεRI
Nt
Ct
B
data
cryo-EM map
ns-EM map
log(I)
q(Å⁻¹)
C
data
1/3 ns-EM +
2/3 cryo-EM
log(I)
q (Å - 1)
D
180°

A

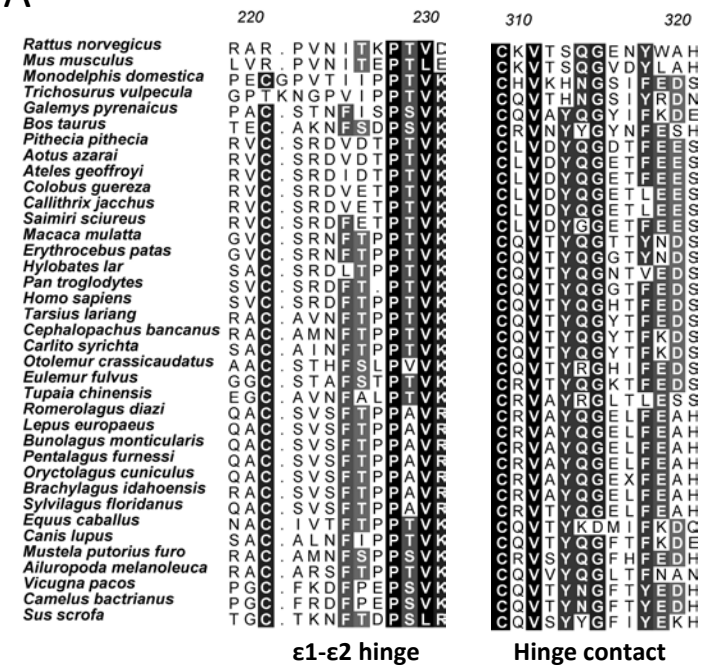
220
230
310
320
Rattus norvegicus
Mus musculus
Monodelphis domestica
Trichosurus vulpecula
Galemys pyrenaicus
Bos taurus
Pithecia pithecia
Aotus azarai
Ateles geoffroyi
Colobus guereza
Callithrix jacchus
Saimiri sciureus
Macaca mulatta
Erythrocebus patas
Hylobates lar
Pan troglodytes
Homo sapiens
Tarsius lariang
Cephalopachus bancanus
Carlito syrichta
Otolemur crassicaudatus
Eulemur fulvus
Tupaia chinensis
Romerolagus diazi
Lepus europaeus
Bunolagus monticularis
Pentalagus furnessi
Oryctolagus cuniculus
Brachylagus idahoensis
Sylvilagus floridanus
Equus caballus
Canis lupus
Mustela putorius furo
Ailuropoda melanoleuca
Vicugna pacos
Camelus bactrianus
Sus scrofa
ε1-ε2 hinge
Hinge contact

B

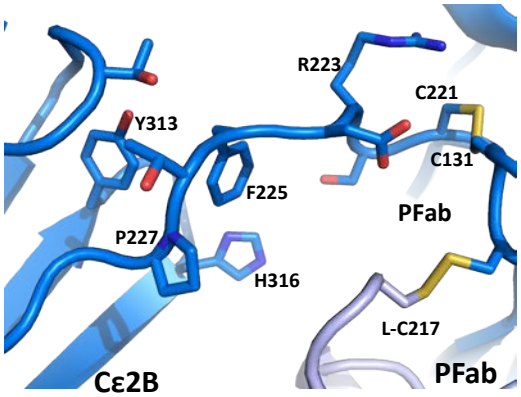
R223
C221
Y313
C131
F225
PFab
P227
H316
L-C217
Cε2B
PFab

C

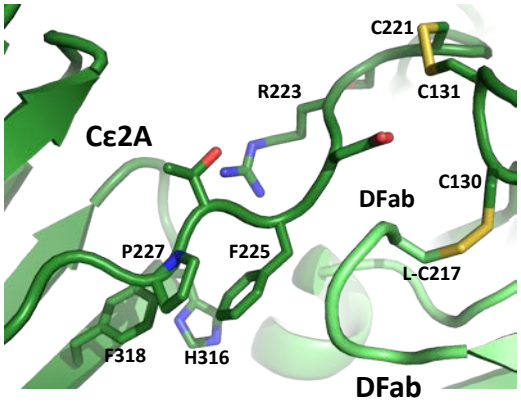
C221
R223
C131
Cε2A
C130
DFab
P227
F225
L-C217
F318
H316
DFab

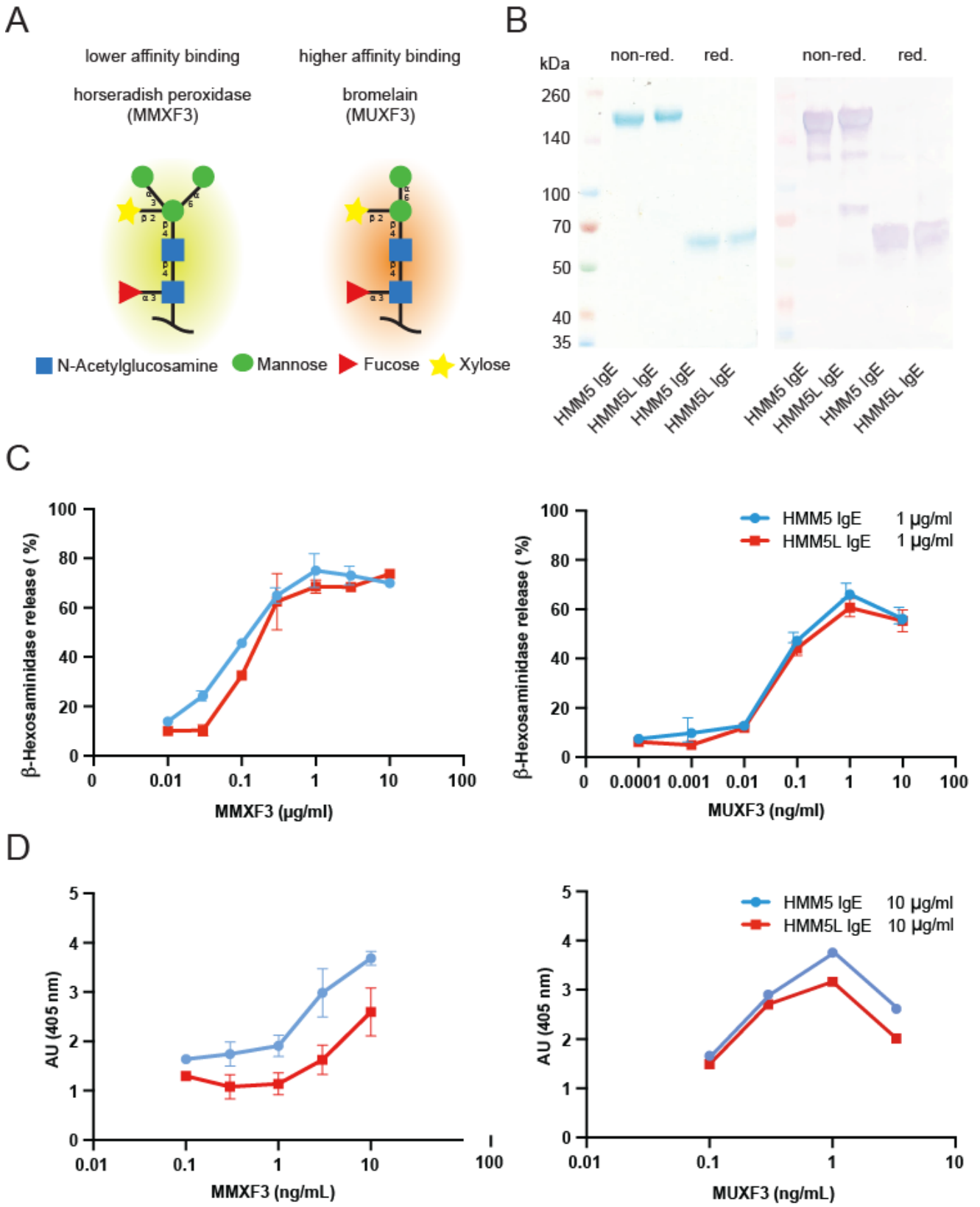
A
lower affinity binding
higher affinity binding
horseradish peroxidase (MMXF3)
bromelain (MUXF3)
N-Acetylglucosamine
Mannose
Fucose
Xylose
B
kDa
non-red.
red.
non-red.
red.
260
140
100
70
50
40
35
HMM5 IgE
HMM5L IgE
HMM5 IgE
HMM5L IgE
HMM5 IgE
HMM5L IgE
HMM5 IgE
HMM5L IgE
C
β-Hexosaminidase release (%)
MMXF3 (µg/ml)
HMM5 IgE 1 µg/ml
HMM5L IgE 1 µg/ml
MUXF3 (ng/ml)
D
AU (405 nm)
MMXF3 (ng/mL)
HMM5 IgE 10 µg/ml
HMM5L IgE 10 µg/ml
MUXF3 (ng/mL)

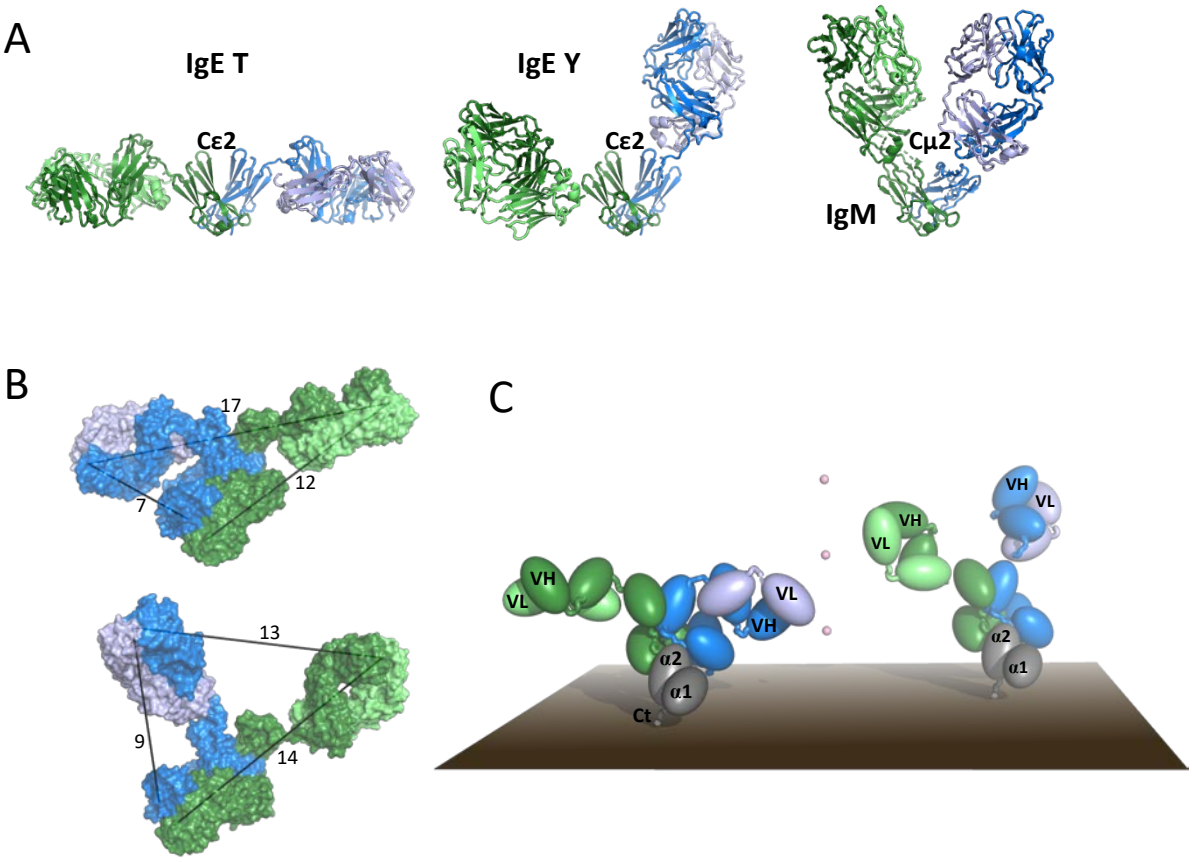
A
IgE T
Cε2
IgE Y
Cε2
Cμ2
IgM
B
17
12
7
13
9
14
C
VH
VL
VL
VH
α2
α1
Ct
VH
VL
VH
VL
α2
α1

Data collection			
Microscope	FEI Titan Krios	No. of frames	40
Magnification	105,000	Defocus range (μm)	0.8-1.8
Voltage (kV)	300	Pixel size (Å)	0.829
Electron exposure (e^{-}/Å^2)	59.16	Symmetry imposed	C1
		No. of micrographs	11015
Deposited data	**Focused**	**Consensus**	
PDB/EMDB entry	8C1B/ EMD-16377	8C1C/EMD-16378	
Atoms	12675 (Hydrogens: 6106)	19267 (Hydrogens: 9284)	
Residues	Protein: 807	Protein: 1237	
Bonds (RMSD)			
Length (Å) (# > 4sigma)	0.007 (0)	0.007 (0)	
Angles (°) (# > 4sigma)	1.257 (16)	1.156 (14)	
MolProbity score	1.42	1.23	
Clash score	3.18	2.40	
Ramachandran plot (%)			
Outliers/ Allowed/ Favored	0.25/4.24/95.51	0.16/3.18/96.66	
Rotamer outliers (%)	0.28	0.00	
ADP (B-factors)			
Iso/Aniso (#)	6569/0	9983/0	
min/max/mean			
Protein	74.57/252.79/131.77	33.87/999.99/346.65	
Ligand	77.58/204.62/119.18	114.39/256.02/176.60	
Data			
Box Lengths (Å)	96.37, 122.28, 103.62	116.06, 122.28, 138.86	
Supplied Resolution (Å)	3.8	4.1	
Resolution Estimates (Å)	Masked Unmasked	Masked Unmasked	
d FSC (half maps; 0.143)	3.8 3.9	4.2 4.2	
d model	3.9 4.0	4.0 4.1	
d FSC model (0/0.143/0.5)	3.6/3.8/4.5 3.7/3.9/6.9	3.9/4.1/6.3 4.0/4.2/7.1	
Map min/max/mean	-3.87/5.25/0.17	-1.18/3.26/0.13	
Model vs. Data			
CC (mask)	0.70	0.71	
CC (box)	0.76	0.87	
CC (peaks)	0.53	0.66	
CC (volume)	0.70	0.70	
Mean CC for ligands	0.74	0.71	

Table 1. Statistics for cryo-EM data collection, refinement and validation. The lower part of the table was prepared with pheinx.validation_cryoem.